ADVANCED OPTICAL MATERIALS
www.advopticalmat.de

Toward Silicon-Matched Singlet Fission: Energy-Level Modifications Through Steric Twisting of Organic Semiconductors

Calvin J. Lee, Ashish Sharma, Naitik A. Panjwani, Isaac M. Etchells, Elham M. Gholizadeh, Jonathan M. White, Paul E. Shaw, Paul. L. Burn, Jan Behrends, Akshay Rao, and David Jones**

Singlet fission (SF) is a potential avenue for augmenting the performance of silicon photovoltaics, but the scarcity of SF materials energy-matched to silicon represents a barrier to the commercial realization of this technology. In this work, a molecular engineering approach is described to increase the energy of the S_1 and T_1 energy levels of diketopyrrolopyrrole derivatives such that the energy-level requirements for exothermic SF and energy-transfer to silicon are met. Time-resolved photoluminescence studies show that the silicon-matched materials are SF active in the solid state, forming a correlated triplet pair ^{1}(TT) – a crucial intermediate in the SF process – as observed through Herzberg-Teller emission from ^{1}(TT) at both 77 K and room temperature. Transient electron paramagnetic resonance studies show that the correlated triplet pair does not readily separate into the unbound triplets, which is a requirement for energy harvesting by silicon. The fact that the triplet pair do not separate into free triplets is attributed to the intermolecular crystal packing within the thin films. Nevertheless, these results demonstrate a promising route for energy-tuning silicon-matched SF materials.

1. Introduction

Singlet fission (SF) is of interest to the optoelectronics community as it provides a potential pathway to overcoming the fundamental Shockley-Queisser (SQ) limit for power conversion efficiencies (PCE) of single-junction photovoltaic (PV) devices.[1] Single-junction silicon solar cells (SSCs) are limited to a PCE of 29.4%, but implementation of a SF layer that splits singlet excitons to two triplets that can be utilized by the silicon cell has been calculated to enhance the PCEs of SSCs up to 34.6%.[2] SF thus represents an attractive route to reduce the cost-per-Watt of solar-generated power, which could lead to improved up-take of SSCs.[3]

Mechanistically, SF is the spin-allowed photophysical evolution of a spin-0 singlet exciton (S_1) on a single chromophore to two spin-1 triplet excitons (T_1) on neighboring chromophores.[4] This has been proposed to occur via an intermediate correlated triplet-pair state (^{1}TT) with overall spin-0 character, which if the energy requirements are met, can diphase and disassociate into free triplets (Equation 1).[5] It should be noted, however, that the role of this species, and whether it is a key intermediate or a hindrance to the SF process, has been hotly debated.[6] If the free triplets possess a combined absolute energy level below that of the first

C. J. Lee, J. M. White, D. Jones
School of Chemistry, Bio21 Institute
University of Melbourne
Parkville, VIC 3010, Australia
E-mail: calvin.lee@unimelb.edu.au; djjones@unimelb.edu.au

A. Sharma, A. Rao
Cavendish Laboratory
University of Cambridge
Cambridge CB3 0HE, UK

N. A. Panjwani, J. Behrends
Berlin Joint EPR Lab, Fachbereich Physik
Freie Universität Berlin
14195 Berlin, Germany

I. M. Etchells, P. E. Shaw, P. L. Burn
Centre for Organic Photonics & Electronics, School of Chemistry and Molecular Biosciences
The University of Queensland
St Lucia, QLD 4072, Australia

E. M. Gholizadeh
School of Chemistry
University of Melbourne
Parkville, VIC 3010, Australia

The ORCID identification number(s) for the author(s) of this article can be found under https://doi.org/10.1002/adom.202301539

DOI: 10.1002/adom.202301539

singlet state (i.e., $E(S_1) > 2\,E(T_1)$) then the overall SF process is exothermic and can proceed favorably from an energetic viewpoint on <100 femtosecond timescales.[5,7]

$$S_1 + S_0 \rightarrow {}^1(TT) \rightarrow T_1 + T_1 \quad (1)$$

The earliest studies on SF chromophores focused primarily on linear acenes like anthracene and tetracene, as well as polycyclic aromatic hydrocarbons (PAHs) like perylene.[8] However interest quickly waned due to the lack of perceived utility in practical applications. This changed in 2004 after the potential contributions of singlet fission materials to the efficiencies of existing PV technologies were identified.[9] Subsequently, computational studies and mechanistic insights have led to the proliferation of potential chromophore designs for efficient singlet fission.[4a,7] However, the practical realization of a diverse library of synthesized SF chromophores – necessary for furthering our understanding the complex mechanisms of singlet fission processes and the development of materials for application in devices – has not yet come to pass, and the pool of synthesized SF-capable chromophores remains limited.[4a,10]

Design guidelines for efficient SF-capable chromophores have been put forward in several publications. From a materials-property standpoint, SF chromophores should be resistant to photochemical and thermal degradation, as well as possess large absorption coefficients and good exciton- and charge-transport properties.[10,11] Energetic considerations revolve around two main criteria: 1) the conditions required to split a singlet exciton into two triplet excitons (i.e., $E(S_1) > 2E(T_1)$ for exothermic SF), and 2) the requirement to suppress the recombination of two unbound triplet excitons.[12] To facilitate practical, SF-augmented solar cells, a third criterion exists: the triplet energy level of the SF chromophore should equal or exceed the PV semiconductor bandgap to facilitate energy transfer between the SF layer and the PV cell (i.e., $E(T_1) > 1.1$ eV in the case of silicon PV).

For practical applications, these requirements immediately rule out many materials, including linear acenes or those designed or selected by computational studies, with these materials often having limited stabilities and/or lack of high visible-region absorptivity's.[13] A high absorptivity is essential as it reduces the thickness of the SF layer required for full absorption of incident light, which in turn mitigates potential losses due to the limited triplet exciton diffusion length. While there are a number of SF-active chromophores that meet the energetic or materials criteria,[14] a much smaller number have been reported with the appropriate triplet energy levels for direct energy transfer to an SSC.[15]

One of the more promising classes of SF-capable materials are the diketopyrrolopyrroles (DPPs),[16] which contain a π-conjugated bicyclic dilactam moiety and have long been used in the paint and organic electronic industries. As such, the properties of DPPs are relatively well-understood, with the materials characterized by high charge mobilities (up to $\approx$10 $cm^2\ V^{-1}\ s^{-1}$),[17] chemical stability, large absorption coefficients and triplet yields, as well as ease of chemical modification.[18] DPPs were first reported to undergo SF by Wasielewski et al. in 2016, where two derivatives – a thiophene-flanked DPP (TDPP) and a phenylthiophene-flanked DPP – were found to exhibit rapid triplet formation and high triplet quantum yields.[14d] Of note was that the calculated T_1 triplet energy levels were found to be at $\approx$1.0 eV, which is below that of the bandgap of silicon.

To circumvent having to perform a bottom-up design of novel SF chromophores ab initio, as has been the case with several ubiquitous SF molecules,[10,13b] we have instead pursued a top-down molecular engineering strategy that modifies the T_1 energy levels of DPP chromophores to match that of the Si bandgap, while still maintaining a sufficient $T_1 - S_1$ energy gap for exothermic SF. This route allows us to take advantage of chromophores with a pre-existing body of knowledge and desirable optoelectronic/material properties, and facilitates the rapid development of SF materials that may have commercial relevance. DPP chromophores are known to be captodatively-stabilized biradicaloids in the ground state (**Figure 1**).[14d,19] That is, their structure is an intermediate between a perfect biradical [$E(S_0) = E(T_1)$] and a closed-shell molecule [$E(T_1) = E(S_1)$] where low electron affinity flanking heteroaromatics are covalently linked to the high electron affinity lactam on either side of a radical center, which leads to enhanced stabilization.[12a,20] This stabilization in turn increases the biradical character of DPPs, thus decreasing the S_0/T_1 energy gap.[21] While most SF molecular design efforts utilize this increase of the chromophore biradical character to lower $E(T_1)$ and thus achieve the $E(S_1) > 2E(T_1)$ condition required for exothermic SF,[13e,22] here we explore an opposite strategy, aiming to decrease the biradical character instead.

It is known that twisting of the bonds between the moieties can decrease the captodative effect and so in turn destabilize the T_1 state – and usually also S_1 – thus raising both the T_1 and S_1 energies (Figure 1a).[12a,23] In this work we introduce steric bulk through the use of chloro- or methyl- groups on the peripheral thiophene moieties to force an out-of-plane twist relative to the lactam core (Figure 1c, DPPC and DPPM respectively). The chloro and methyl groups hinder co-planarization of the thiophene moiety with the lactam core, and thus favor the closed-shell form (left-hand side, Figure 1b) over the quinoidal form.

Through the investigation of the two compounds via steady–state spectroscopic measurements of thin films, we find that our structural modifications for DPPC and DPPM indeed resulted in increased T_1 and S_1 energy levels (relative to an unmodified TDPP chromophore). These energy levels fulfill the requirements for exothermic singlet fission, with the energy levels of the triplet exciton well-matched to the Si bandgap. Transient absorption (TA) and time-resolved photoluminescence (PL) studies demonstrate that photoexcitation of thin films produces species with ^{1}(TT) character on a picosecond timescale. However, transient electron paramagnetic resonance (trEPR) spectroscopy did not reveal signatures of triplets formed from SF, suggesting that the ^{1}(TT) species does not spontaneously dissociate into free triplets. We conjecture that the solid-state packing of the two new DPPs does not readily facilitate the formation of free triplets, and propose solutions for next-generation chromophores that can overcome these limitations while still harnessing our successful energy-tuning molecular engineering strategy.

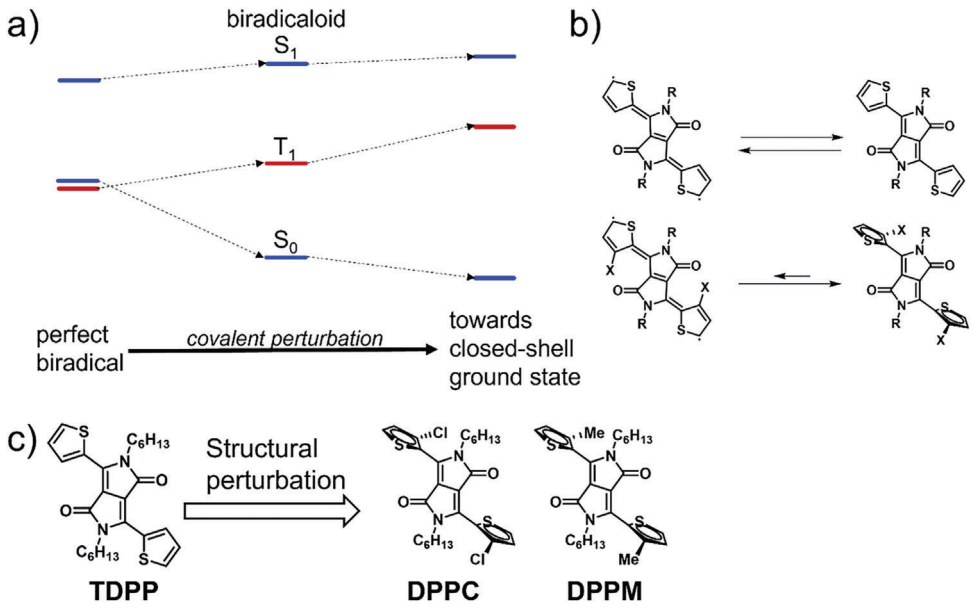

Figure 1. a) Schematic representation of biradical and biradicaloid energy levels, with the latter an intermediate between a perfect biradical and a closed-shell molecule (Adapted with permission.[21b] Copyright 2022, John Wiley and Sons), b) biradicaloid-quinoidal resonance structures of DPP-based chromophores, and c) molecular engineering route for energy level modifications used in this publication.

2. Results and Discussion

2.1. Synthesis and Materials Properties

The synthesis of the DPP analogues followed a two-step pathway, as outlined in **Scheme 1**. The highly insoluble 3,6-diaryl lactam core was formed first, with this then *N*-alkylated using a linear *n*-hexyl chain to impart solubility for ease of solution-processing. The lactam cores of the two compounds were synthesized via a modified version of the widely-used base-promoted pseudo-Stobbe condensation of aryl nitriles with succinic acid esters to form DPPs.[18d] We employed a sodium hydride dispersion in *tert*-amyl alcohol to readily form the sodium alkoxide base. We found that for the synthesis of the precursor lactams corresponding to DPPM and DPPC, poor yields of ≈10%–20% were obtained. This is not unexpected, as it has been shown in the literature that sterically hindered aryl nitriles have adverse effects on lactam condensations,[18d,24] potentially reducing the yield by up to a factor of 10.[25]

N-Alkylation of the lactam cores was carried out using a modified literature procedure,[26] where we utilized caesium carbonate as the base and *n*-hexyl iodide as the electrophile. These conditions were used to maximize reaction yields through minimization of the formation of the unwanted *O*-alkylated products. However, *O*-alkylation was still an issue and occurred more readily than with non-hindered DPP analogues, with greater than a 50% yield of the *O*-alkylated material obtained. The synthetic procedure and structural characterization can be found in the

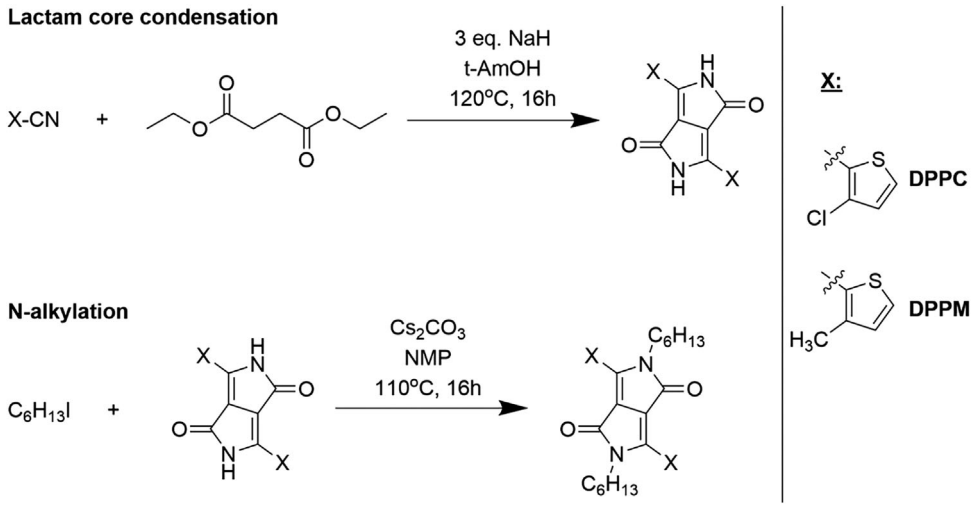

Scheme 1. General synthetic pathway to the two DPP-based chromophores.

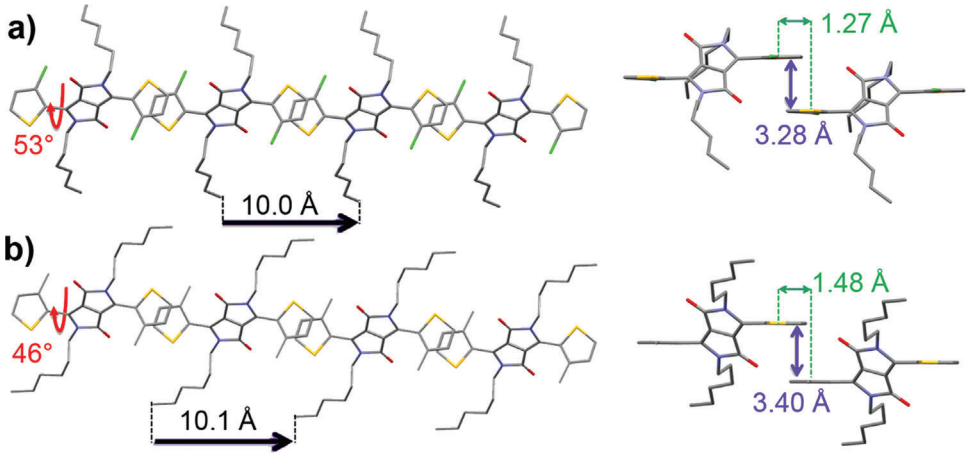

Figure 2. Comparison of the crystal structures of a) DPPC and b) DPPM with the thiophene-lactam dihedral angles (red), horizontal lactam core translational offset (black), horizontal centroid-to-centroid π-overlap offset (green) and vertical π-stacking distances (purple) labelled. Structures are shown as a top-down (left) and side-on (right) view. Hydrogens are omitted for clarity.

Supporting Information. Both molecules possessed good thermal stabilities with decomposition temperatures of ≈250 °C for both DPPC and DPPM, as determined by thermogravimetric analysis (TGA) under nitrogen (Figure S7, Supporting Information). These temperatures are similar to those reported for other non-planar DPPs.[27]

2.2. Structural Characterization

Single-crystal X-ray diffraction was used to characterize the new DPPs. The substituents on the β-position of the thiophene ring of DPPC and DPPM (**Figure 2**) result in elongated C-C bonds between the lactam core and the flanking thiophene (1.47 and 1.46 Å for DPPC and DPPM, respectively) relative to TDPP (1.42 Å), which is consistent with a shift away from a quinoidal form. Notably, both also exhibited significant twisting of peripheral thiophene rings relative to the lactam core, with dihedral angles of 53° and 46°, respectively. This in turn significantly alters the π-stacking behavior and degree of electronic overlap between neighboring chromophores relative to the DPP chromophores featured in the work of Wasielewski. In that work, the importance of close π-stacking between chromophores and its impact on the electronic-coupling-dependent SF process was highlighted, with SF found to occur in planar TDPP, but not in a phenyl-flanked DPP derivative (PDPP), where there was a greater π-stacking distance (3.9 Å) in the single-crystal structure.[14d]

As seen in the "top-down" view in Figure 2, although DPPC and DPPM possess close π-stacking distances of <3.4 Å (well within the chromophore-chromophore proximity required for SF),[28] the significant dihedral angle twists have driven the π-overlap to be between the thiophenes on neighboring molecules, resulting in large (≈10 Å) horizontal translations observed between the lactam cores. In contrast, TDPP and PDPP exhibit thiophene-lactam overlap with a correspondingly smaller horizontal translations of ≈3.5 Å. We discuss the implications of this solid-state packing later in this work.

An extended view of the crystal lattices can be seen in **Figure 3**. DPPC and DPPM pack in a herringbone arrangement, with DPPC adopting a tetrameric arrangement of four π-stacked sheets driven by the thiophene-thiophene π-stacking and intermolecular Cl-O interactions. Likewise, for DPPM its thiophene-thiophene π-stacking interactions is a primary driver behind the formation of herringbone sheets. Comparison of the calculated powder diffraction patterns derived from the single-crystal structures of DPPC and DPPM to the radial averages from the

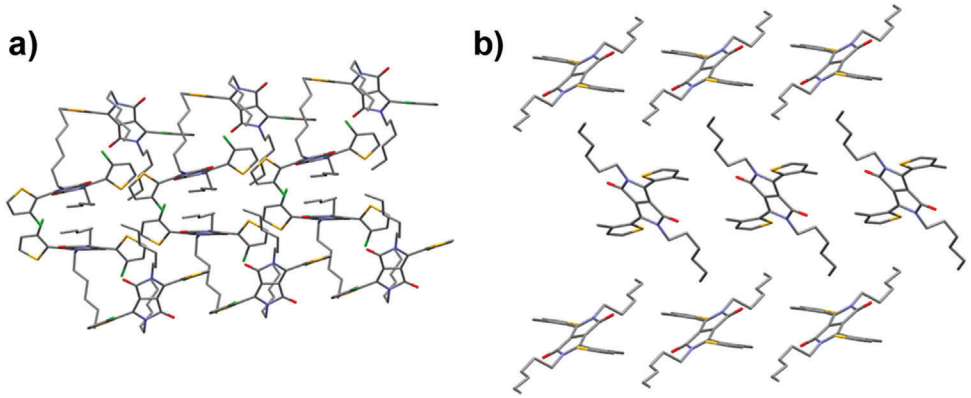

Figure 3. Comparison of crystal structures showing extended lattice packings of a) DPPC and b) DPPM exhibiting herringbone packing motifs.

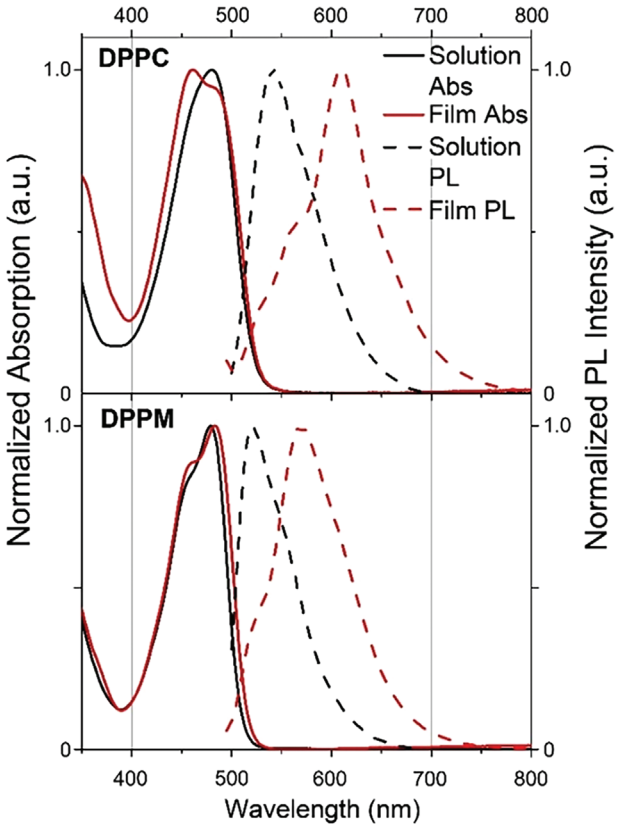

Figure 4. Steady–state normalized absorption (solid line) and emission (dotted line) spectra of DPPC and DPPM in dilute chloroform solution (black) and as spin-coated films on glass substrates (red).

experimental GIWAXS scattering patterns (Figure S8, Supporting Information) show good agreement between the two measurements, suggesting that the bulk morphologies of the thin films are consistent with the crystalline packing observed in the single-crystal data – which is to say, comprised of horizontal sheets of π-stacked structures.

2.3. Steady–State Optical Properties

Steady state absorption and emission spectra of both materials were recorded in dilute chloroform solutions and as spin-coated thin films deposited from chloroform solution (**Figure 4**), with the relevant information summarized in **Table 1**. DPPC and DPPM have similar absorption properties and between solution and film, which suggests limited aggregation or insignificant effects of local molecular order on the absorption cross section in the solid state. The solid-state photoluminescence (PL) spectra for both DPPC and DPPM had little structure, while the ≈50 nm emission peak redshift relative to the solution spectra is indicative of interchromophore interactions in the solid state. Thus, the solid-state PL measurements indicate that the increased dihedral angles between the lactam core and the peripheral thiophene moieties have not completely hindered the interchromophore interactions in the solid state.

A comparison of the absorption spectra of the two materials relative to TDPP (Table 1), show that the new materials have a blue shifted peak maximum translating, in turn, to increases in the optical gaps (E_g^{Opt}) of ≈450 to 500 meV for DPPC and DPPM relative to TDPP.

Photoluminescence studies were also performed in the near-IR spectral region of 950–1600 nm. While no emission was recorded at room temperature, cooling the thin films to 77 K led to emission appearing for both materials. We assigned this emission to phosphorescence from the triplet state T_1, and hence calculate T_1 energy levels of 1.16 and 1.15 eV from the phosphorescence onset for DPPC and DPPM, respectively (see Figure S9 for further details, Supporting Information). By using the optical gap determined from the absorption onset λ_{ons}^{Abs} to approximate the first excited singlet state S_1 (see Figure S10 for further details, Supporting Information), we thus show that the twisting introduced into the new DPP analogues destabilizes both the T_1 and S_1 energy levels for DPPC and DPPM. Furthermore, the relative energy levels should be appropriate for exothermic singlet fission and, if free triplets were generated, sufficiently energy matched to allow direct energy transfer to a silicon semiconductor.

2.4. Time-Resolved Photoluminescence and Quantum Yields

Time-correlated single-photon counting (TCSPC) measurements were used to determine the decay kinetics of the excited singlet state of the chromophores in solution and thin film (Figure S11, Supporting Information), with the fitted decay lifetimes summarized in **Table 2**. The solution-state measurements exhibited single exponential decays, while the films featured biexponential decays with an additional short-lived component. This suggests an excited-state deactivation pathway accessible in the thin-films due to intermolecular interactions that are not present in solution, which is a minimum requirement for solid-state singlet fission. The introduction of intermolecular interactions in the films are supported by the photoluminescence quantum yields (PLQYs) of the materials, with PL quenching (40%–50%, relative to solution) observed for both materials in the solid state.

Table 1. Optical and electrochemical properties of DPPC, DPPM and TDPP.

	$\lambda_{max}^{Abs,\,sol}$ (nm)	ϵ_{max} (M^{-1} cm^{-1})	$\lambda_{max}^{Abs,\,film}$ (nm)	$\lambda_{ons}^{Abs,\,film}$ (nm)	$\lambda_{max}^{Ems,\,film}$ (nm)	S_1^{film} (eV)	T_1^{film} (eV)	$E(S_1\text{-}2T_1)$ (eV)
DPPC	480	1.14×10^4	490	527	610	2.35	1.16	0.03
DPPM	480	1.59×10^4	482	519	564	2.39	1.15	0.09
TDPP[a)]	548	2.76×10^4	610	650	-	1.90	0.95	0

[a)] Taken from Harnett et al.[14d]

Table 2. Summary of time-resolved photoluminescence kinetics and PLQYs.

	Lifetime	Contribution	PLQY
DPPC		Solution	
	6.24 ± 0.01 ns	-	36%
		Film	
	1.66 ± 0.05 ns	0.77	22%
	4.91 ± 0.10 ns	0.23	
DPPM		Solution	
	4.45 ± 0.01 ns	-	67%
		Film	
	2.67 ± 0.07 ns	0.80	37%
	3.95 ± 0.12 ns	0.20	

2.5. ^{1}(TT) Photoluminescence Studies

The use of temperature-dependent PL studies has emerged as a powerful approach to provide positive confirmation of singlet fission via identification of the formation of a ^{1}(TT) state. The existence of this state in previously-studied chromophores has been debated due in part to its spectral similarity to free triplets in transient absorption spectroscopy,[29] as well as its inability to be detected via paramagnetic-response techniques that are commonly used for studying SF systems due to its spin-0 nature. Recent publications on a variety of SF-active materials, including a study on DPP derivatives, have succeeded in directly probing this state, and do so via the observation of ^{1}(TT) emission.[5,29b,30] ^{1}(TT) emission in SF systems is usually observed as red-shifted delayed emission with strong vibronic features, a result of Herzberg-Teller (HT) vibronic intensity borrowing process that allows mixing of the dark ^{1}(TT) state with a bright S_1 state.[31] Here this results in emission with structure that is similar to the singlet emission. This distinguishes it from excimer-derived emission, which is typically broad, featureless and with a much larger redshift. Furthermore, the excited state lifetime of the ^{1}(TT) and excimer states are significantly different, as discussed in the next paragraph.

Emission consistent with Herzberg-Teller emission can be observed in the time-resolved normalized PL spectra of both DPPM (**Figure 5**) and DPPC (**Figure 6**) in the solid state. To clarify the behavior seen here, we also include the non-normalized spectra (Figure S14, Supporting Information). For DPPM, at 77 K a clear ≈10 nm redshift in the PL profile can be observed (Figure 5a) over the first 50 ns, which is consistent with the evolution from the S_1 state to a new emissive species consistent with Herzberg-Teller emission from a ^{1}(TT) state. This behavior is different from that reported in Mauck et al. for the room-temperature emission from a TDPP excimer, which decayed over the much shorter timescale of a 0.2–2.4 ns.[14d] It is important to note that 100 ns after excitation (Figure 5b) there is a ≈10 nm blueshift in the PL emission spectrum, with this delayed emissive species matching the profile of the prompt PL, signifying a repopulation of the S_1 state from the ^{1}(TT) state. This result provides further evidence to distinguish the intermediate state from an excimer. The relatively quick timeframe over which the repopulation of the S_1 occurs suggests it proceeds through reverse-SF of the ^{1}(TT) state. Interestingly, ^{1}(TT) emission may also be occurring at room temperature (Figure 5c), a phenomenon previously seen in both functionalized acenes and DPPs.[5] The PL at room temperature is significantly weaker relative to that observed at 77 K, which results in a low signal-to-noise ratio in the first 30 ns of the measurement, and casts ambiguity on the presence of a spectral shift.

For DPPC, at 77 K there is a clear change in the shape of the PL with an apparent suppression of the S_1 0-0 peak at 560 nm over the first 50 ns after excitation relative to the ^{1}(TT) 0–1 peak at 600 nm (Figure 6a). At longer time delays (≈100 ns after excitation, Figure 6b) there is a recovery of the S_1 0-0 peak intensity, which suggests that there is a repopulation of the S_1 state from the recombining of a ^{1}(TT) state in a similar fashion as to that observed for the DPPM film. However, unlike DPPM there appears to be a contribution from S_1 emission at all times and so the emission spectrum of the ^{1}(TT) state cannot be fully isolated. Mirroring the behavior observed at 77 K, after excitation at room temperature we can see an evolution of a ^{1}(TT) state (Figure 6c), followed by recovery to the S_1 state, and is likely another example of temperature-independent ^{1}(TT) emission. Thus, DPPC and DPPM represent the second reported example of direct ^{1}(TT) emission observed in a DPP-based thin film.[29b]

Using PL spectra of DPPC and DPPM thin films at 77 K at different time delays, we were also able to isolate the individual spectral features of the S_1 and ^{1}(TT) states, and from these estimate the S_1 and ^{1}(TT) energy levels from the respective emission onsets (for further details see Figure S15, Supporting Information). These energy levels are displayed in **Figure 7** and were used to estimate the ^{1}(TT) binding energies. As the Herzberg-Teller mechanism suppresses the 0-0 peak position, the ^{1}(TT) energy levels have been calculated by adding one vibrational quantum (0.12 eV) to the 0–1 peak position of the ^{1}(TT) emission. Note that there is also some degree of uncertainty in the calculation of the S_1 energy levels due to the spectral overlap between species and the subsequent difficulty in fitting the emission onsets. This likely accounts for the differences in energy levels calculated from the room-temperature, steady–state PL, but is irrelevant for the ^{1}(TT) binding energy calculations.

2.6. Transient Electron Paramagnetic Resonance Spectroscopy

The PL studies clearly show the formation of the correlated triplet pair state ^{1}(TT). However, for SF-augmented solar cells to be realized the triplet pair must undergo dissociation into free triplets. Recent studies by Maity et al. showed that their DPP based molecule, HR-TDPP-TEG,[29b] in a J-aggregate morphology undergoes partial SF to form the ^{1}(TT) but does not further evolve to give free triplets. Instead, the long-lived triplets in their study were shown to come from the more conventional mechanisms of spin-orbit coupling mediated intersystem crossing (SO-ISC). Based on the weak trEPR signal intensity, the SO-ISC triplet yield was considered to be relatively low. Therefore, to detect and characterize any long-lived states formed in DPPC and DPPM films, we perform trEPR spectroscopy at a temperature of 50 K.

The DPPC and DPPM films showed an extremely weak signal in the trEPR measurement, and we therefore present the

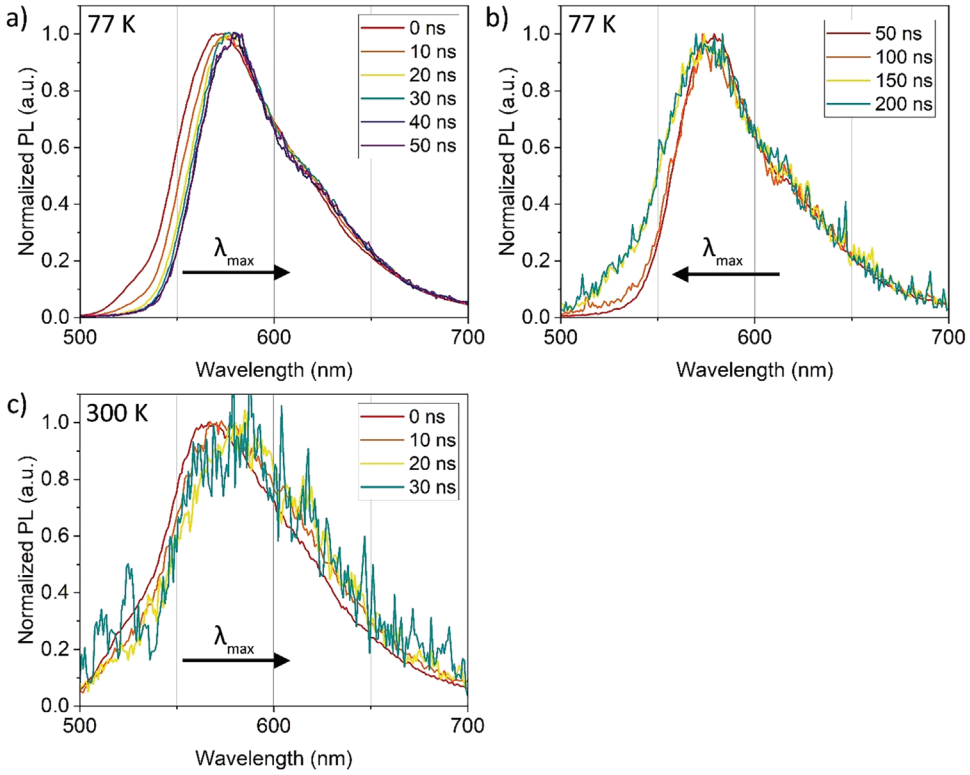

Figure 5. Time-resolved normalized photoluminescence spectra of spin-coated DPPM thin films obtained at 77 K (a,b) and at 300 K (c). Black arrows highlight the direction of peak maxima shifts as a function of time.

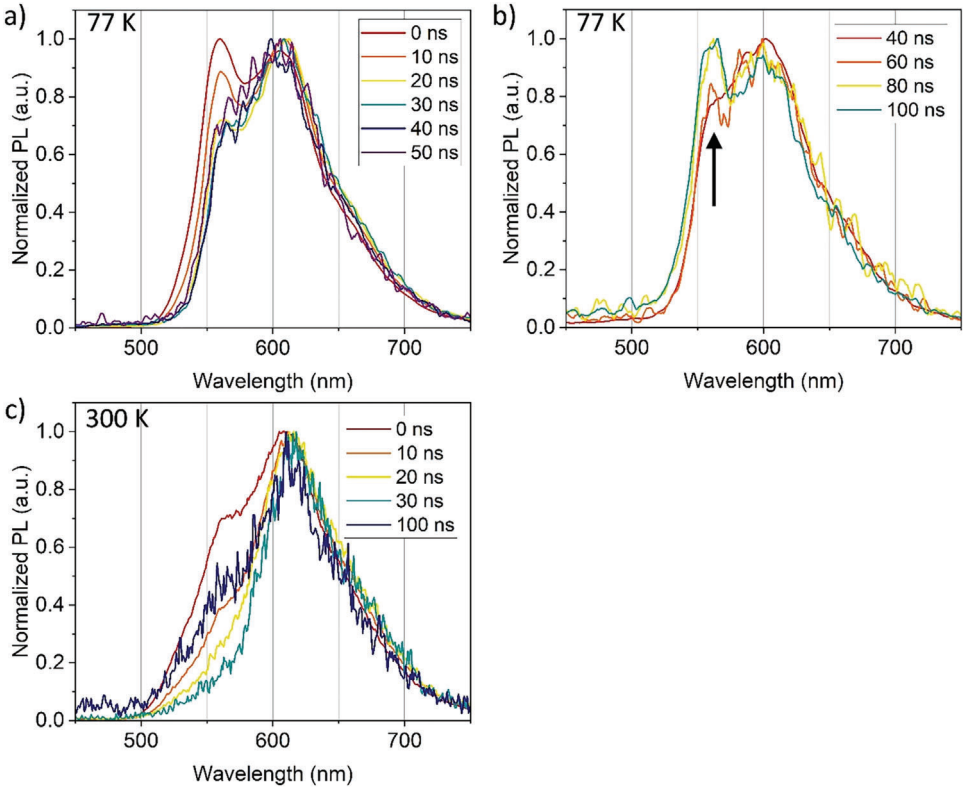

Figure 6. Time-resolved normalized photoluminescence spectra of spin-coated DPPC thin films obtained at 77 K (a,b) and at 300 K (c). The black arrow highlights the increase of peak intensity as a function of time.

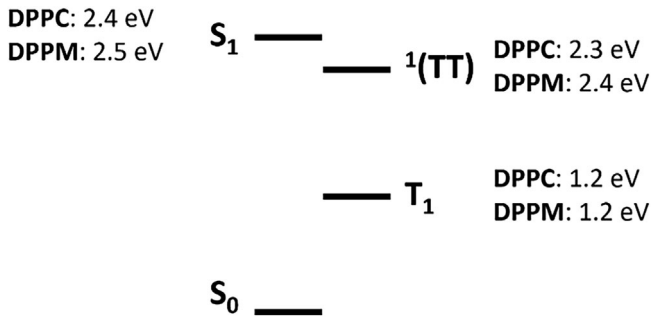

Figure 7. Energy levels of DPPC and DPPM determined from PL spectra of thin films at 77 K.

time-averaged spectra from 0.2–3.0 µs for improved signal-to-noise (full 2D trEPR maps are shown in Figure S13, Supporting Information). The time-averaged spectrum shown in **Figure 8** for both films show an extremely broad triplet feature with an electron spin polarization (ESP) pattern of *aea/eae* where *a* is enhanced absorption and *e* is emission. The spectra were modelled using the MATLAB toolbox EasySpin,[32] with zero-field splitting parameters of $D \approx 1750–1850$ MHz and $|E| \approx 270–320$ MHz with the uncertainty in D and E due to the weak signal. Our E value is consistent with those reported for triplets formed on other TDPP based molecules. However, the D value for DPPC and DPPM is much larger than that measured for triplets formed on TDPP via charge recombination in a TDPP/$PC_{70}BM$ blend sample, c.f. ≈1550 MHz,[33] and for SO-ISC triplets recently reported in HR-TDPP-TEG films, c,f. $D \approx 1150–1250$ MHz.[29b] The much larger D parameter needed to simulate the experimental data indicates that triplet excitons formed on DPPC and DPPM are much more localized, as would be expected with the twist between the thiophene rings and the lactam core, which leads to a more localized electron spin density.

To understand the mechanism for the formation of the observed triplets, we look again to the ESP pattern. For free triplets arising from the ^{1}(TT) state, the high field eigenstates (T_-, T_0, T_+) are directly populated and assuming preferential population of the T_0 sublevel this would result in an ESP of either *aee/aae* for $D > 0$ or *eaa/eea* for $D < 0$.[34] However, if the triplet state is formed via SO-ISC then the population of the triplet sublevels is due to selective population of the zero-field eigenstates namely T_x, T_y, T_z. The ESP observed for both DPPC and DPPM of *aea/eae* is consistent with populations based on zero-field eigenstates and therefore the mechanism for triplet formation in the materials of this study is SO-ISC, with the low intensity due to the process being inefficient due to a lack of strong spin-orbit coupling. The difference in the trEPR spectrum of DPPC and DPPM is due to differences in the relative populations of the T_x, T_y, T_z sublevels, for DPPC the relative sublevel populations are 0.6, 0.0, 0.4 and for DPPM it is 0.5, 0.0, 0.5. However, the critical result is that the free triplets formed have not come from the ^{1}(TT) state. Finally, in addition to the triplets arising from SO-ISC we also see a narrow signal at $g \approx 2$, which is an emissive transition for DPPC and absorptive transition for DPPM. This state is likely a charge transfer (CT) state similar to that observed for HR-TDPP-TEG films.[29b]

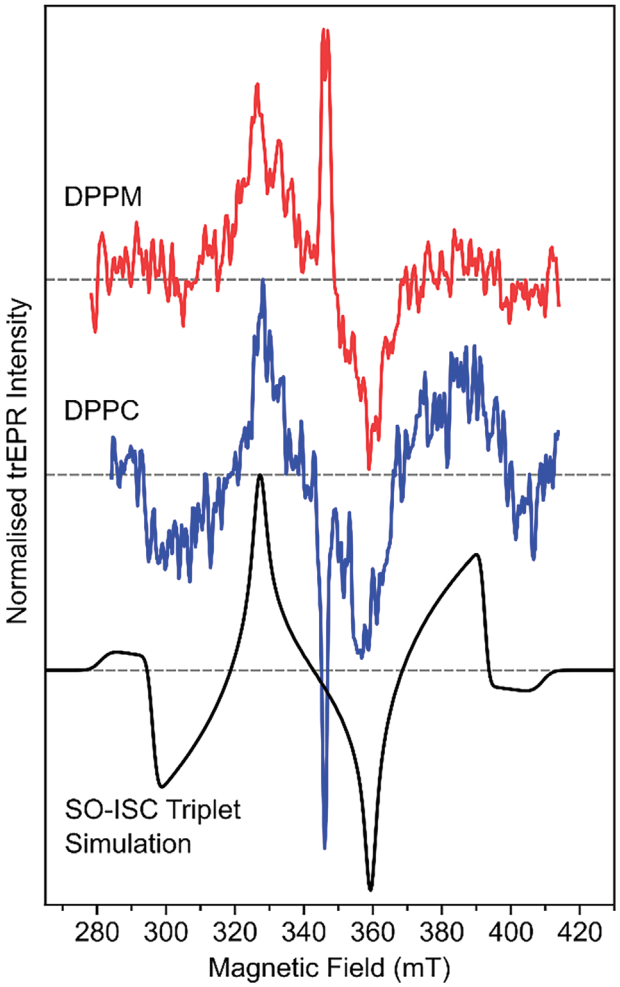

Figure 8. Transient EPR spectra of (Red) DPPM and (Blue) DPPC films measured at 50 K after excitation at 490 and 480 nm respectively. Experimental spectra are time averaged from 0.2–3.0 µs. (Black) Simulation showing a representative EPR spectrum of triplets formed via SO-ISC with $D = 1800$ MHz and $|E| = 300$ MHz and triplet sublevel population of $P_{x,y,z} = 0.6, 0.0, 0.4$.

2.7. Transient Absorption Spectroscopy

Transient absorption is often used to probe the generation and evolution of excited state species. Based on the time-resolved PL and the EPR measurements we would expect to see spectral features corresponding to a singlet exciton population generated upon photoexcitation followed by conversion to the correlated triplet pair, as well as features from free triplets generated from ISC. Picosecond (ps) and nanosecond (ns) transient absorption measurements on DPP films cast on sapphire substrates were undertaken to probe the excited-state dynamics of the materials, with the corresponding spectra observed in **Figure 9**. Analogous films cast on glass were obtained (Figure S16, Supporting Information) but not utilized in our analysis due to overexaggerated PIA-like signal lifetimes attributed to transient thermal modulation from the optical pump.[29b,35] For both DPPC and DPPM (Figure 5a,b) immediately after excitation we observe overlapping positive ground-state bleach (GSB) signals between

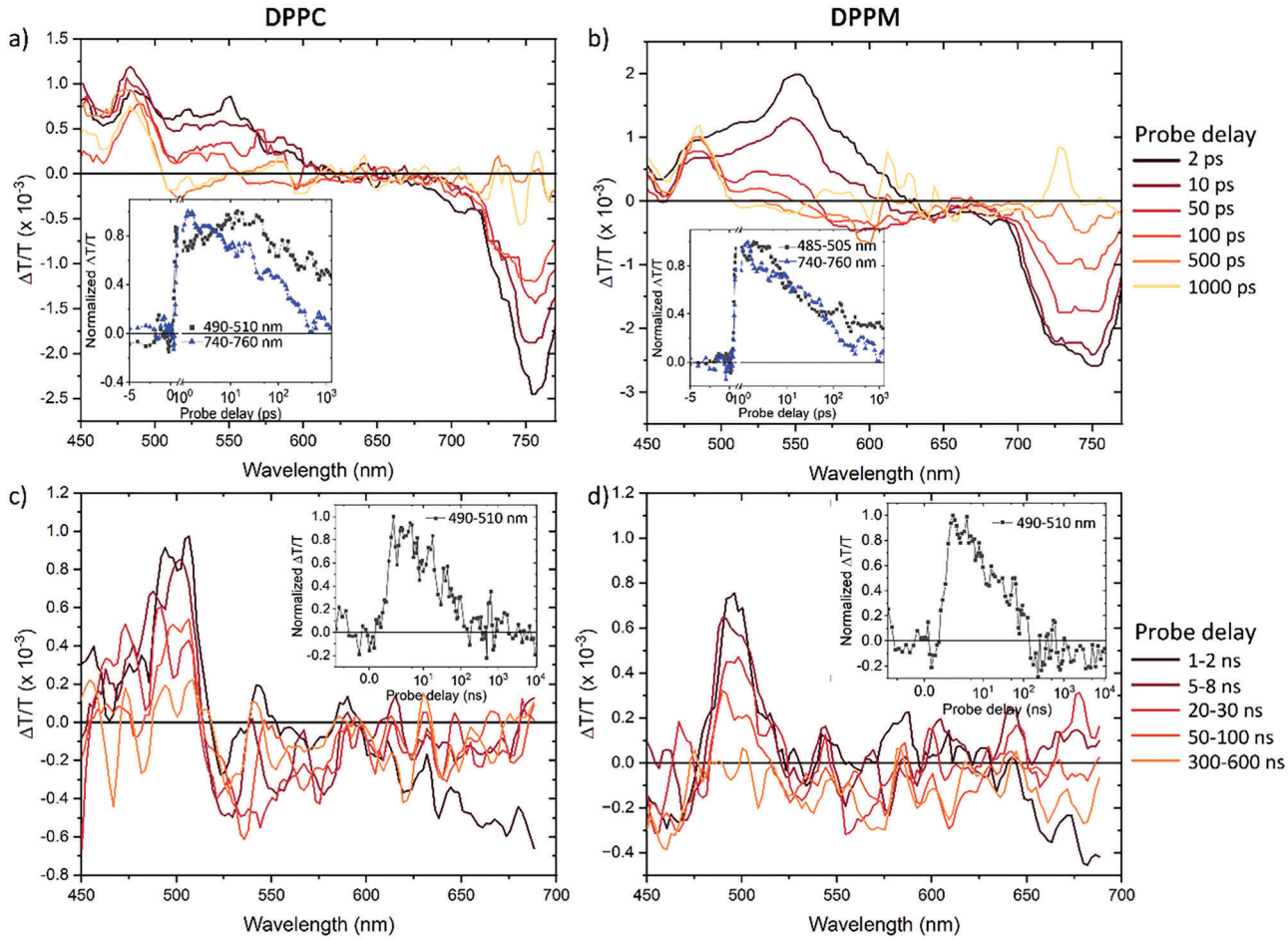

Figure 9. ps-TA spectra (top, excitation at 400 nm) and ns-TA spectra (bottom, excitation at 355 nm) for thin films of DPPC (a,c) and DPPM (b,d) coated on a sapphire substrate. Inset: kinetics traces for the ground-state bleach (grey trace) and singlet exciton (blue trace) species.

480–500 nm and positive stimulated emission (SE) signals between 500–600 nm. Both these features possess similar spectral position and profiles as the steady–state absorption and emission, respectively. We also observe a weak negative photoinduced absorption (PIA) signal ≈500–525 nm, attributed to triplet-triplet absorptions in other DPP materials in the literature,[29b,36] as well as a strong PIA signal ≈750 nm, attributed to the singlet excited state (S_1).[36,37]

The GSB signal for DPPC at 500 nm is best fitted to a triexponential model (Figure 5a, inset) with an initial rise in the first 15 ps followed by a biexponential decay with lifetimes of $\tau = 33$ ps and 60.2 ns (the latter of which is obtained from fitting the ns-TA data, Figure 5c inset). The singlet PIA feature at 750 nm decays with a major, rapid component ($\tau = 50$ ps, 80%) and a minor, slower component ($\tau = 500$ ps, 20%). For clarity, the time constants associated with these species have been tabulated in **Table 3**. The substantial overlap of the PIA at 520 nm with the SE feature obscures its presence at earlier (<100 ps) timeframes, complicating the kinetic resolution of the involved species. This weak absorption feature assigned to the triplet resulting from an ISC process (see tr-EPR study) persists into the nanosecond regime and can be observed in the ns-TA spectra. However, the poor signal-to-noise ratio complicates modelling.

Table 3. Time constants of kinetic traces from transient absorption studies.

	DPPC	DPPM
Ground-state bleach	$\tau_1 = 15 \pm 10$ ps $\tau_2 = 33 \pm 16$ ps $\tau_3 = 60.2 \pm 15$ ns	$\tau_1 = 12.7 \pm 2.2$ ps $\tau_2 = 49.9 \pm 12.7$ ns
Singlet exciton	$\tau_1 = 50 \pm 10$ ps $\tau_2 = 503 \pm 110$ ps	$\tau_1 = 51 \pm 12$ ps $\tau_2 = 1.3 \pm 0.8$ ns

For DPPM (Figure 5b,d), the GSB feature at 495 nm is fitted with a biexponential decay with $\tau = 12.7$ ps and 49.6 ns. Here we also observe a weak triplet PIA at 580 nm that is overlapped with the SE feature, as well as a strong singlet exciton PIA at 750 nm. Again, similarly to DPPC the singlet exciton PIA at 750 nm undergoes a biexponential decay with a rapid major ($\tau = 51$ ps, 90%) and slower minor ($\tau = 1300$ ps, 10%) component.

The analysis of the 500–525 nm triplet-like PIA feature is difficult due to the overlap of this feature with the positive SE feature in the ps-TA spectra. As such it was not possible to elucidate the lifetimes or triplet yields. However, from solution-state triplet sensitization studies of DPPC (Figure S12 and Note S1, Supporting Information) we observe the T_1 absorption in DPPC shares

the same spectral region with the 500–525 nm PIA feature, suggesting that free triplets are responsible for this absorption in the solid state. As indicated by the transient EPR studies it is unlikely that these free triplets are derived from a SF process, but instead arise from intersystem crossing.

3. Discussion

This work reports the successful modification of the triplet and singlet energy levels of a singlet fission chromophore as a step toward facilitating exoergic energy transfer to a silicon semiconductor. However, it seems clear that the SF process these new chromophores falters at the final hurdle, as we do not observe disassociation of the key SF intermediate, ^{1}(TT), into free triplets. In this discussion we bring together the results from the transient photoluminescence, transient EPR and transient absorption studies to construct a cohesive understanding of the photophysical processes involved and explore the reasons behind the absence of SF-derived free triplet generation.

DPPC and DPPM do not differ significantly in their excited-state behaviors. Upon photoexcitation the majority of the excited singlet population in thin films of the materials decay non-radiatively – as inferred from the solid-state PLQYs – either to the ground or ^{1}(TT) state. From the TA and time-resolved PL data we estimate the prompt fluorescence rate to be ≈0.5 ns for DPPC and 1.3 ns for DPPM. Tr-EPR studies further suggest that the generation of triplets from ISC represents a minor decay pathway from S_1. From the ^{1}(TT) photoluminescence studies we can estimate the ^{1}(TT) state for both materials to have a lifetime in between 10^1–10^2 ns, which is analogous to the long GSB recovery term obtained from the ns-TA studies. The PL studies also demonstrated a repopulation of the S_1 state from recombination of ^{1}(TT). However, even in the case of DPPC, where this emission is observed at room temperature, we do not detect any delayed florescence from the TCSPC measurements.

From the energy levels determined from the tr-PL studies we were able to estimate the ^{1}(TT) binding energies [E_b ^{1}(TT)] with respect to the free triplets, where E_b $^1(TT) = E(^1TT) - E(T_1+T_1)$, and find this value to be ≈50–100 mEV for DPPC and DPPM. The absence of free triplets is then particularly curious considering this low binding energy, as this energy is comparable to the values (typically ≈30–100 meV) reported for chromophores that readily generate SF-derived free triplets.[30a,38] Recent work has shown that apart from the dimer, perylene oligomers can generate free triplets via the ^{1}(TT) pair state.[39] In the case of the perylene dimer, the triplet pair instead underwent triplet recombination to repopulate the S_1 state in a similar fashion to that observed from the tr-PL studies of DPPC and DPPM. Triplet pair dephasing is known to require sufficient space over which the triplet pair can diffuse, with the increase in entropy facilitating free triplet formation.[40] Examining the single-crystal structures of DPPC and DPPM, we see that while there is a close ≈0.3 nm π-stacking distance between the peripheral thiophenes, the lactam cores have a relatively large spatial offset of ≈1 nm. A rationalization for the lack of free triplet formation could thus be that while the solid-state packing geometry for DPPC and DPPM facilitates ^{1}(TT) generation localized between two adjacent DPP chromophores, the relative lack of electronic overlap with neighboring molecules hinders ^{1}(TT) diffusion into spatially separated triplets.

While the inability of DPPC and DPPM to undergo ^{1}(TT) dissociation into free triplets is unfortunate, the demonstrated ability to raise the energy levels of a singlet fission chromophore is not, and we present a further route for singlet fission molecular design that can potentially overcome this hurdle while still harnessing these energy-level modifications. We have previously utilized a molecular π-bridge with self-assembling properties to covalently link two triplet host chromophores,[14g] and believe that this structural motif can impose greater electronic overlap and molecular order on chromophores with sterically-bulky components like DPPC and DPPM. This, then, would theoretically afford both higher singlet/triplet energy levels for silicon bandgap matching, while also affording the greater spatial freedom for entropic assistance for triplet pair dephasing

4. Conclusion

In this work we explored the use of a molecular engineering strategy to reduce the biradical character of a singlet fission capable chromophore, where sterically bulky moieties were used to disrupt the captodative stabilization of a biradical center. This was performed with the overall goal of raising the energy of the T_1 and S_1 states to a level that would enable energy transfer to a silicon semiconductor – a property lacking in the vast majority of extant singlet fission chromophores. Two novel DPP analogues, DPPC and DPPM, were synthesized. Low-temperature phosphorescence measurements allowed us to estimate the T_1 energy levels for both chromophores to be at 1.1 eV, thus elevating DPPC and DPPM to the handful of SF materials energetically compatible with silicon. SF to a correlated triplet pair state ^{1}(TT) was observed through spectroscopic measurements, however, the generated triplet pair did not undergo dissociation into free triplets. The triplets observed in the transient EPR measurements were only consistent with SO-ISC and were extremely weak (indicative of a low ISC rate). We believe that the low disassociation yield of the correlated triplet pair can be attributed to crystal packing that is sub-optimal for triplet delocalization, reducing the overall entropic favorability for decorrelation. Nevertheless, this work demonstrates a useful approach to molecular design for SF materials energy-matched to silicon. We expect that this strategy can be applied to other promising molecular classes with desirable materials properties, and lead to the rapid expansion of the physical SF material library needed to move the field forward.

5. Experimental Section

Materials and Material Characterization: Details of the synthesis and characterization of DPPC, DPPM and their respective precursors were reported in the Supporting Information.

Unless noted, all materials were reagent grade and used as received without further purification. The precursors to DPPC, thiophenes **2** and **3**, were synthesized and purified according to reported literature procedures.[41] The precursor to DPPM, 3-methylthiophene-2-carbonitrile, was bought from Thermo Fisher Scientific and used as received. Chromatographic separations were performed using standard column methods over silica (Merck 9385 Kieselgel). ^{1}H NMR and ^{13}C NMR spectra were carried out on a 400 or 600 MHz Bruker spectrometer. All NMR

data was referenced to the residual chloroform signal at 7.26 ppm. ESI mass spectrometry was performed on a Thermo Fisher Exactive™ Plus Orbitrap Mass Spectrometer instrument. Elemental analyses were undertaken by the Elemental Microanalysis Service at Macquarie University using a Vario MICRO cube elemental analyser (Elementar Analysensysteme GmbH, Germany). Thermal gravimetric analysis (TGA) experiments were carried out with a Mettler Toledo TGA/SDTA851e.

Structural Characterization: Crystals for diffraction studies were grown by slow evaporation from methanol. Single-crystal data was gathered from the MX1 beamline at the Australian Synchrotron.[42] The structures of DPPC and DPPM had been deposited in the Cambridge Crystallographic Data Centre database (CCDC 2241674 and 2241675). This data can be obtained free of charge from The Cambridge Crystallographic Data Centre via www.ccdc.cam.ac.uk/data_request/cif

Samples for GIWAXS studies were prepared by spin-coating 20 mg mL^{-1} solutions of the DPP materials in chloroform onto Si wafers at 1000 rpm for 30 s. The Si wafers had been sonicated in acetone and *iso*-propanol for 15 min each followed by 30 min of UV/Ozone treatment. The GIWAXS experiments were performed at the Australian Synchrotron on the SAXS/WAXS beamline under vacuum.[43] A Pilatus 200 K detector was used for 2D diffraction pattern collection. The energy of the incident beam was 15 keV at a range of incident angles from $\theta = 0.02 - 0.20°$. The sample-to-detector range was 30 cm. Data from the GIWAXS experiments was analyzed using a customized version of NIKA 2D based in IgorPro.[44]

Optical Characterization: For the optical measurements solution-state studies were carried out in degassed toluene or chloroform, and solid-state samples were spin-coated on fused silica or sapphire substrates obtained from Ossila. Spin-coating conditions were identical to those used to form the films for GIWAXS characterization. The Si or sapphire substrates were sonicated in acetone and *iso*-propanol for 15 min each followed by 30 min of UV/Ozone treatment.

Steady–state UV–vis absorption spectra were measured on a Cary 3500 UV–vis Spectrometer over the photon energy range 1.55–4.13 eV. Steady–state photoluminescence spectra were collected using a Cary Eclipse Spectrophotometer.

Time-resolved photoluminescence spectra were recorded using an Andor iStar iCCD system with a Kymera 193i monochromator connected to the light collecting collimator fiber optic placed 90° to the sample compartment. The sample was excited with an Opolette 355 LD (355 nm, 10 ns, 5 μJ $pulse^{-1}$) Nd:YAG laser.

Phosphorescence Measurements: Steady–state phosphorescence PL spectra were obtained on a home-built setup, which was equipped with a Horiba detector (Horiba Jobin Yvon iHR320) and an amplified InGaAs photodetector (Electro-Optical System). Excitation of the samples were performed using a supercontinuum laser (NKT Photonics, SuperK Extreme& Varia) at 480 nm. The measurements were performed at 77 K by cooling the samples using a liquid nitrogen cryostat (Oxford Instruments, Optistat DN). Emission was recorded in the range of 1000–1600 nm. A 550 nm long-bandpass filter was used on emission path to remove the third harmonic of the excitation. The power density of the excitation on the sample was 1.5×10^{-4} W cm^{-2}.

Transient Absorption Measurements: The transient absorption measurements in the picosecond (ps-TA) and nanosecond (ns-TA) time-domains were performed using a custom setup. For the ps-TA, the laser source was a Ti:sapphire amplifier system (Spectra-Physics Solstice) operating at a frequency of 1 kHz. A part of the 1 kHz pulse was frequency doubled using a BBO crystal to generate the pump beam (400 nm). Another part of the output from the Ti:sapphire system was focused on a CaF_2 crystal to generate broadband probe beams in the visible region. The pump beam was delayed with respect to the probe beam by passing it through a mechanical delay stage (Thorlabs DDS300-E/M).

For the ns-TA, the pump was generated by the third harmonic (355 nm) of a Qswitched Nd:YVO4 (1 ns pump length, Advanced Optical Technologies Ltd AOT-YVO-25QSPX). The probe beam was generated with a LEUKOS Disco 1 UV supercontinuum laser (STM-1-UV, 1 kHz) and was delayed electronically with respect to the pump.

To measure the TA signal, the pump and probe beams were overlapped on the sample and focused into an imaging spectrometer (Andor, Shamrock SR 303i). The beams were detected using a pair of linear image sensors (Hamamatsu, G11608) driven and read out at the full laser repetition rate by a custom-built board from Stresing Entwicklungsburo. A chopper (500 Hz) was used to have pump-on and pump-off periods during all measurements, which enabled the system software to calculate differential transmission, $\Delta T/T$.

Transient EPR Characterization: Transient EPR experiments were performed on a laboratory-built X-band (9.7 GHz) continuous wave spectrometer together with a Bruker MD5 dielectric ring resonator with optical access. Optical excitation was provided by an Opta OPO (Model 355 I, 410–700 nm) pumped by a Spectra-Physics QuantaRay LabSeries 150 Nd:YAG laser, with an incident pulse energy of ≈2.3 mJ (at 490 nm for DPPM film sample) and ≈1.7 mJ (at 480 nm for DPPC film sample), a pulse length of 7 ns, and operating at 10 Hz. Excitation at each wavelength also included a depolarizer (DPP25-A, Thorlabs) to avoid polarization effects. The temperature was controlled using a Lakeshore 332 temperature controller and a laboratory-built helium flow cryostat. Transients were recorded as the static magnetic field was swept and continuous-wave microwave irradiation was applied (samples were measured with a microwave power of 0.53 mW). EPR samples were prepared in the following manner: Solutions of DPPM and DPPC were prepared in a nitrogen atmosphere glovebox, in anhydrous toluene at a concentration of 10 mg mL^{-1} and stirred until all material was dissolved. Solutions were then transferred to 2.9 mm inner diameter (3.9 mm outer diameter) quartz EPR tubes and transferred to a pumping station (using a custom adapter that keeps the sample tube in the inert glovebox atmosphere) before being freeze-pump-thawed twice at a pressure of 2×10^{-3} mbar to degas the solution. The solution was then evaporated under vacuum to leave a film on the inner wall of the EPR tube. The tube was left to pump to a pressure of 4.5×10^{-4} mbar before being flame sealed. Experimental spectra presented in Figure 8 were smoothed using the data smooth function in EasySpin, which makes a moving average.[32] The window for the moving average was set to 3 points and the default binomial weighting method was used.

Supporting Information

Supporting Information is available from the Wiley Online Library or from the author.

Acknowledgements

This program had been supported by the Australian Government through the Australian Renewable Energy Agency (ARENA), either directly or through the Australian Centre for Advanced Photovoltaics. The Australian Government, through ARENA, was supporting Australian research and development in solar photovoltaic and solar thermal technologies to help solar power become cost competitive with other energy sources. The views expressed herein are not necessarily the views of the Australian Government, and the Australian Government does not accept responsibility for any information or advice contained herein. The authors also acknowledge financial support from the German Research Foundation (DFG grant number BE 5126/6-1). P.L.B. is a UQ Laureate Fellow.

Open access publishing facilitated by The University of Melbourne, as part of the Wiley - The University of Melbourne agreement via the Council of Australian University Librarians.

Conflict of Interest

The authors declare no conflict of interest.

Data Availability Statement

The data that support the findings of this study are available in the supplementary material of this article.

Keywords

diketopyrrolopyrroles, organic semiconductors, organic electronics, photoenergy conversion, singlet fission, synthesis

Received: June 29, 2023
Revised: September 17, 2023
Published online: October 12, 2023

[1] M. A. Green, *Prog. Photovoltaics* **2001**, *9*, 123.
[2] B. Daiber, K. van den Hoven, M. H. Futscher, B. Ehrler, *ACS Energy Lett.* **2021**, *6*, 2800.
[3] N. S. Lewis, *Science* **2016**, *351*, aad1920.
[4] a) M. B. Smith, J. Michl, *Chem. Rev.* **2010**, *110*, 6891; b) B. J. Walker, A. J. Musser, D. Beljonne, R. H. Friend, *Nat. Chem.* **2013**, *5*, 1019.
[5] H. L. Stern, A. Cheminal, S. R. Yost, K. Broch, S. L. Bayliss, K. Chen, M. Tabachnyk, K. Thorley, N. Greenham, J. M. Hodgkiss, J. Anthony, M. Head-Gordon, A. J. Musser, A. Rao, R. H. Friend, *Nat. Chem.* **2017**, *9*, 1205.
[6] C. B. Dover, J. K. Gallaher, L. Frazer, P. C. Tapping, A. J. Petty, M. J. Crossley, J. E. Anthony, T. W. Kee, T. W. Schmidt, *Nat. Chem.* **2018**, *10*, 305.
[7] S. Ito, T. Nagami, M. Nakano, *J. Photochem. Photobiol. C* **2018**, *34*, 85.
[8] W. G. Albrecht, H. Coufal, R. Haberkorn, M. E. Michel-Beyerle, *Physica Status Solidi* **1978**, *89*, 261.
[9] A. Nozik, R. Ellingson, O. Micic, J. Blackburn, P. Yu, J. Murphy, M. Beard, G. Rumbles, presented at Proceedings of the 27th DOE Solar Photochemistry Research Conference **2004**.
[10] T. Ullrich, D. Munz, D. M. Guldi, *Chem. Soc. Rev.* **2021**, *50*, 3485.
[11] A. J. Baldacchino, M. I. Collins, M. P. Nielsen, T. W. Schmidt, D. R. Mccamey, M. J. Y. Tayebjee, *Chemical Physics Reviews* **2022**, *3*, 021304.
[12] a) J. Wen, Z. Havlas, J. Michl, *J. Am. Chem. Soc.* **2015**, *137*, 165; b) E. A. Buchanan, J. Michl, *J. Am. Chem. Soc.* **2017**, *139*, 15572.
[13] a) J. E. Anthony, *Angew. Chem., Int. Ed.* **2008**, *47*, 452; b) J. C. Johnson, J. Michl, *Top. Curr. Chem.* **2017**, *375*, 80; c) A. Rao, R. H. Friend, *Nat. Rev. Mater.* **2017**, *2*, 17063; d) Y. L. Lin, M. A. Fusella, O. V. Kozlov, X. Lin, A. Kahn, M. S. Pshenichnikov, B. P. Rand, *Adv. Funct. Mater.* **2016**, *26*, 6489; e) D. Padula, Ö. H. Omar, T. Nematiaram, A. Troisi, *Energy Environ. Sci.* **2019**, *12*, 2412.
[14] a) S.o Kawata, Y.-J. Pu, A. Saito, Y. Kurashige, T. Beppu, H. Katagiri, M. Hada, J. Kido, *Adv. Mater.* **2016**, *28*, 1585; b) S. Masoomi-Godarzi, M. Liu, Y. Tachibana, L. Goerigk, K. P. Ghiggino, T. A. Smith, D. J. Jones, *Adv. Energy Mater.* **2018**, *8*, 1801720; c) E. A. Margulies, J. L. Logsdon, C. E. Miller, L. Ma, E. Simonoff, R. M. Young, G. C. Schatz, M. R. Wasielewski, *J. Am. Chem. Soc.* **2017**, *139*, 663; d) P. E. Hartnett, E. A. Margulies, C. M. Mauck, S. A. Miller, Y. Wu, Y.i-L. Wu, T. J. Marks, M. R. Wasielewski, *J. Phys. Chem. B* **2016**, *120*, 1357; e) K. J. Fallon, P. Budden, E. Salvadori, A. M. Ganose, C. N. Savory, L. Eyre, S. Dowland, Q. Ai, S. Goodlett, C. Risko, D. O. Scanlon, C. W. M. Kay, A. Rao, R. H. Friend, A. J. Musser, H. Bronstein, *J. Am. Chem. Soc.* **2019**, *141*, 13867; f) J. Hu, K.e Xu, L. Shen, Q. Wu, G. He, J.-Y.u Wang, J. Pei, J. Xia, M. Y. Sfeir, *Nat. Commun.* **2018**, *9*, 2999; g) S. Masoomi-Godarzi, M. Liu, Y. Tachibana, V. D. Mitchell, L. Goerigk, K. P. Ghiggino, T. A. Smith, D. J. Jones, *Adv. Energy Mater.* **2019**, *9*, 1901069.
[15] a) F. S. Conrad-Burton, T. Liu, F. Geyer, R. Costantini, A. P. Schlaus, M. S. Spencer, J. Wang, R. H. Sánchez, B. Zhang, Q. Xu, M. L. Steigerwald, S. Xiao, H. Li, C. P. Nuckolls, X. Zhu, *J. Am. Chem. Soc.* **2019**, *141*, 13143; b) S. W. Eaton, L. E. Shoer, S. D. Karlen, S. M. Dyar, E. A. Margulies, B. S. Veldkamp, C. Ramanan, D. A. Hartzler, S. Savikhin, T. J. Marks, M. R. Wasielewski, *J. Am. Chem. Soc.* **2013**, *135*, 14701.
[16] T. Mukhopadhyay, A. J. Musser, B. Puttaraju, J. Dhar, R. H. Friend, S. Patil, *J. Phys. Chem. Lett.* **2017**, *8*, 984.
[17] M. Desu, S. Sharma, K.-H. Cheng, Y.u-H. Wang, S. Nagamatsu, J.-C. Chen, S. S. Pandey, *Org. Electron.* **2023**, *113*, 106691.
[18] a) C. Fu, P. J. Beldon, D. F. Perepichka, *Chem. Mater.* **2017**, *29*, 2979; b) C. B. Nielsen, M. Turbiez, I. Mcculloch, *Adv. Mater.* **2013**, *25*, 1859; c) A. Tang, C. Zhan, J. Yao, E. Zhou, *Adv. Mater.* **2017**, *29*, 1600013; d) M. Grzybowski, D. T. Gryko, *Adv. Opt. Mater.* **2015**, *3*, 280.
[19] a) R. Rausch, M. I. S. Röhr, D. Schmidt, I. Krummenacher, H. Braunschweig, F. Würthner, *Chem. Sci.* **2021**, *12*, 793; b) Y. Li, l. li, Y. Wu, Y. Li, *J. Phys. Chem. C* **2017**, 121.
[20] H. G. Viehe, Z. Janousek, R. Merenyi, L. Stella, *Acc. Chem. Res.* **1985**, *18*, 148.
[21] a) W. Wang, L. Ge, G. Xue, F. Miao, P. Chen, H. Chen, Y. Lin, Y. Ni, J. Xiong, Y. Hu, J. Wu, Y. Zheng, *Chem. Commun.* **2020**, *56*, 1405; b) Z. Havlas, J. Michl, *Isr. J. Chem.* **2016**, *56*, 96.
[22] a) M. Nakano, *Chem. Rec.* **2017**, *17*, 27; b) T. Minami, M. Nakano, *J. Phys. Chem. Lett.* **2012**, *3*, 145.
[23] J. Michl, *J. Am. Chem. Soc.* **1996**, *118*, 3568.
[24] M. Pieczykolan, B. Sadowski, D. T. Gryko, *Angew. Chem., Int. Ed.* **2020**, *59*, 7528.
[25] H. Langhals, T. Potrawa, H. Nöth, G. Linti, *Angew. Chemie Internat. Ed. Eng.* **1989**, *28*, 478.
[26] F. Pop, J. Humphreys, J. Schwarz, L. Brown, A. Van Den Berg, D. B. Amabilino, *New J. Chem.* **2019**, *43*, 5783.
[27] J. David, M. Weiter, M. Vala, J. Vynuchal, J. Kucerík, *Dyes Pigm.* **2011**, *89*, 137.
[28] a) T. Nagami, S. Ito, T. Kubo, M. Nakano, *ACS Omega* **2017**, *2*, 5095; b) R. Casillas, M. Adam, P. B. Coto, A. R. Waterloo, J. Zirzlmeier, S. R. Reddy, F. Hampel, R. Mcdonald, R. R. Tykwinski, M. Thoss, D. M. Guldi, *Adv. Energy Mater.* **2019**, *9*, 1802221.
[29] a) D. G. Bossanyi, M. Matthiesen, S. Wang, J. A. Smith, R. C. Kilbride, J. D. Shipp, D. Chekulaev, E. Holland, J. E. Anthony, J. Zaumseil, A. J. Musser, J. Clark, *Nat. Chem.* **2021**, *13*, 163; b) N. Maity, W. Kim, N. A. Panjwani, A. Kundu, K. Majumder, P. Kasetty, D. Mishra, R. Bittl, J. Nagesh, J. Dasgupta, A. J. Musser, S. Patil, *Nat. Commun.* **2022**, *13*, 5244.
[30] a) C. K. Yong, A. J. Musser, S. L. Bayliss, S. Lukman, H. Tamura, O. Bubnova, R. K. Hallani, A. Meneau, R. Resel, M. Maruyama, S. Hotta, L. M. Herz, D. Beljonne, J. E. Anthony, J. Clark, H. Sirringhaus, *Nat. Commun.* **2017**, *8*, 15953; b) H. L. Stern, A. J. Musser, S. Gelinas, P. Parkinson, L. M. Herz, M. J. Bruzek, J. Anthony, R. H. Friend, B. J. Walker, *Proc. Natl. Acad. Sci. USA* **2015**, *112*, 7656.
[31] G. Orlandi, W. Siebrand, *J. Chem. Phys.* **1973**, *58*, 4513.
[32] S. Stoll, A. Schweiger, *J. Magn. Reson.* **2006**, *178*, 42.
[33] E. Salvadori, N. Luke, J. Shaikh, A. Leventis, H. Bronstein, C. W. M. Kay, T. M. Clarke, *J. Mater. Chem. A* **2017**, *5*, 24335.
[34] a) M. J. Y. Tayebjee, S. N. Sanders, E. Kumarasamy, L. M. Campos, M. Y. Sfeir, D. R. Mccamey, *Nat. Phys.* **2017**, *13*, 182; b) L. R. Weiss, S. L. Bayliss, F. Kraffert, K. J. Thorley, J. E. Anthony, R. Bittl, R. H. Friend, A. Rao, N. C. Greenham, J. Behrends, *Nat. Phys.* **2017**, *13*, 176.
[35] a) A. Rao, M. W. B. Wilson, S. Albert-Seifried, R. Di Pietro, R. H. Friend, *Phys. Rev. B* **2011**, *84*, 195411; b) S. Albert-Seifried, R. H. Friend, *Appl. Phys. Lett.* **2011**, *98*, 223304.
[36] A. M. Levine, C. Schierl, B. S. Basel, M. Ahmed, B. A. Camargo, D. M. Guldi, A. B. Braunschweig, *J. Phys. Chem. C* **2019**, *123*, 1587.
[37] A. M. Levine, G. He, G. Bu, P. Ramos, F. Wu, A. Soliman, J. Serrano, D. Pietraru, C. Chan, J. D. Batteas, M. Kowalczyk, S. J. Jang, B. L. Nannenga, M. Y. Sfeir, E. H. R. Tsai, A. B. Braunschweig, *J. Phys. Chem. C* **2021**, *125*, 12207.

[38] a) M. Fumanal, C. Corminboeuf, *Chem. Mater.* **2022**, *34*, 4115. b) S. Lukman, J. M. Richter, L.e Yang, P. Hu, J. Wu, N. C. Greenham, A. J. Musser, *J. Am. Chem. Soc.* **2017**, *139*, 18376.
[39] N. V. Korovina, N. F. Pompetti, J. C. Johnson, *J. Chem. Phys.* **2020**, *152*, 040904.
[40] R. D. Pensack, E. E. Ostroumov, A. J. Tilley, S. Mazza, C. Grieco, K. J. Thorley, J. B. Asbury, D. S. Seferos, J. E. Anthony, G. D. Scholes, *J. Phys. Chem. Lett.* **2016**, *7*, 2370.
[41] A. El Kassmi, F. Fache, M. Lemaire, *Synth. Commun.* **1994**, *24*, 95.
[42] N. P. Cowieson, D. Aragao, M. Clift, D. J. Ericsson, C. Gee, S. J. Harrop, N. Mudie, S. Panjikar, J. R. Price, A. Riboldi-Tunnicliffe, R. Williamson, T. Caradoc-Davies, *J. Synchro. Radia.* **2015**, *22*, 187.
[43] N. M. Kirby, S. T. Mudie, A. M. Hawley, D. J. Cookson, H. D. T. Mertens, N. Cowieson, V. Samardzic-Boban, *J. Appl. Crystallogr.* **2013**, *46*, 1670.
[44] E. Gann, X. Gao, C.-a. Di, C. R. McNeill, *Adv. Funct. Mater.* **2014**, *24*, 7211.

